SAND2018-9626C

An intrinsic kinetics model to predict complex ash effects (ash film, dilution, and vaporization) on pulverized coal char burnout in air (O_2/N_2) and oxy-fuel (O_2/CO_2) atmospheres

Yanqing Niu[a,*], Siqi Liu[a], Christopher R. Shaddix[b], Shi'en Hui[a]

[a] State Key Laboratory of Multiphase Flow in Power Engineering, Department of Thermal Engineering, School of Energy and Power Engineering, Xi'an Jiaotong University, 710049, Shaanxi, China

[b] Combustion Research Facility, Sandia National Laboratories, Livermore, CA 94550, USA

Corresponding author:

Yanqing Niu, State Key Laboratory of Multiphase Flow in Power Engineering, Department of Thermal Engineering, School of Energy and Power Engineering, Xi'an Jiaotong University, 710049, Shaanxi, China

Email: yqniu85@mail.xjtu.edu.cn; Tel:+086-18161847667

Colloquium: Solid Fuels Combustion

Paper Length (Method 1)		**Words**
Total		**6200**
Main text		3480
Equations	(11+0)* 7.6*1+(2+0)*7.6*2	114
Nomenclature	(28+4)*7.6	243
References	(25+2)*2.3*7.6	472
Table 1	(8+2)*7.6*2	152
Figure 1	(38+10)*2.2*1+11	117
Figure 2	(98+10)*2.2*2+27	502
Figure 3	(52+10)*2.2*1+18	154
Figure 4	(85+10)*2.2*1+18	227
Figure 5	(147+10)*2.2*2+48	739

No color reprints necessary

Abstract: During coal combustion, char chemical reaction is the slowest step, particularly in the last burnout stage, where the char consists of small amounts of carbon in a predominant ash framework. Existing kinetics models tend to deviate from experimental measurements of late char burnout due to the incomplete treatment of ash effects. Ash can improve pore evolution through vaporization, hinder oxygen transport by forming an ash film, and reduce active carbon sites and available surface per unit volume by penetrating into the char matrix. In this work, a sophisticated kinetics model, focusing on these three ash evolution mechanisms (ash vaporization, ash film, and ash dilution) during pulverized coal (PC) char combustion, is developed by integrating them into a thorough mechanistic picture. Further, a detailed comparison of the three distinct ash effects on PC char conversion during air (O_2/N_2) and oxy-fuel (O_2/CO_2) combustion is performed. For the modeled coal, the mass of ash vaporization is approximate 3 orders less than the mass of ash remaining, which participates in ash dilution and ash film formation, both in O_2/N_2 and O_2/CO_2 atmospheres. The influence of these phenomena on burnout time follows the order: ash dilution $>$ ash film $>$ ash vaporization. The influence of ash vaporization on burnout time is minor, but through interactions with the ash dilution and ash film forming processes it can have an impact at high extents of burnout, particularly in O_2/CO_2 atmospheres. In O_2/N_2 atmospheres the residual ash predominately exists as an ash film, whereas it mainly exists as diluted ash in the char matrix in O_2/CO_2 atmospheres. The residual ash particle is encased by a thick film when the ash film forming fraction is high (low ash dilution fraction). These results provide in-depth insights into the conversion of PC char and further utilization of the residual ash.

Keywords: ash; char combustion; ash film; ash dilution; ash vaporization

Nomenclature:

Symbols			
A	pre-exponent factor (g/s/cm^2/atm^n)	Q	burning rate (g/cm^2/s)
CO	carbon monoxide	P	pressure (atm)
CO_2	carbon dioxide	R	radius (cm)
d	diameter (cm)	$\bar{r}$	average radius of the pore channel (cm)
D	diffusion coefficient (cm^2/s)	R	ideal gas constant (8.314J/mol/K)
E	activation energy (kJ/mol)	S_g	internal specific surface area (cm^2/g$_C$)
F	mass fraction (wt.%)	T	temperature (K)
m, M	mass (g), molar mass (g/mol)	X	fraction of ash forming an ash film
MO_n	metal oxides	Y	ash content
MO_{n-1}	metal suboxides and metals	V	vaporization rate (mol/s), volume (cm^3)
N	inclusions number per char particle	$\triangle t$	time duration (s)
Greek alphabet			
α	mode-of-burning parameter	τ	tortuosity
ρ	mass density (g/cm^3)	σ_c	constriction factor
η, η'	effectiveness factor	θ	porosity
δ	thickness of ash film		volume fraction of inclusion
Subscript			
0	initial	eff	effective
a	ash	ex	external
a,f	porous ash	tot	total
af	ash film	g, l, s	gas, liquid, solid
a,n	nonporous ash	inc	inclusion
c	carbon	i, j	computational shell number
cc	char core	vap	vaporization
Superscript			
eq	equilibrium	n	intrinsic reaction order

1. Introduction

During char particle combustion in pulverized coal (PC) furnaces, the particle may undergo full oxygen diffusion control due to fast chemical reaction at high temperatures at the beginning of combustion, combined chemical reaction and oxygen diffusion control at intermediate stages of burnout, and complete chemical reaction control due to slow reaction within the char-ash matrix during final burnout [1]. Char conversion is generally the slowest step in the process of coal particle combustion, particularly in the last burnout stage, where the char consists of small amounts of carbon in a predominant ash framework [2]. Numerous studies have addressed char conversion rates based on carbon reactivity. However, far fewer studies have considered the influence of ash mineral matter, which affects the number of active carbon sites per volume, pore structure, and oxygen diffusion [2, 3], and thereby also plays an important role in char conversion [2, 4-6].

Ash minerals in coal exist either as inherent, organically bound, atomically dispersed impurities or as adventitious mineral matter. During combustion, the former (including Hg, As, alkali and alkaline earth metals, etc) easily vaporizes and diffuses out of the char matrix, while refractory elements (e.g. Si, Al, and Fe) partially volatilize. These volatilized mineral constituents are essential for the formation of ultra-fine particulate matter (PM). However, for most coals the overwhelming majority of the inorganic matter remains associated with the char particles and ultimately exits the boiler as residual fly ash [1, 7-11]. The ash transformations can have important effects on char thermal conversion, and they become increasingly important during burnout [5]. ***Ash vaporization*** not only promotes pore structure generation and development [1, 5], but also reduces the available ash within the particle that may impact carbon consumption, such as by the generation of low-melting alkali salts and consequently pore plugging by molten ash [11].

Until now, numerous char burning kinetics models have been developed, and some of these have considered the influence of ash [2, 12, 13]. The Carbon Burnout Kinetic (CBK) model, developed by Hurt et al. [2], integrates an apparent char oxidation kinetics model, thermal annealing, and ash inhibition. This model was the first attempt

to provide a description of ash inhibition on char combustion during burnout. As reported by Hurt and Davis [6] for char particles from two US high-volatile bituminous coals, the apparent kinetics model shows small errors for carbon conversions below 50%, but by 70% conversion the reactivity has decreased by a factor of two. Meanwhile, the estimated deactivation from thermal annealing is too small to match the observed level of reactivity loss [2]. Therefore, it is apparent that the influence of ash inhibition on char conversion must be accounted for to accurately describe the complete burnout process [2]. Existing models such as CBK have accounted for ash inhibition using a simple ***ash film*** model, in which it is assumed that the ash liberated during char combustion accumulates on the outer surface of the particle and acts to hinder oxygen diffusion to the encapsulated char core [2, 3, 6]. The ash film model undoubtedly is applicable to fluidized bed combustion, in which larger fuel particles burn at moderate temperatures [14, 15]. However, for PC particle combustion the ash film model appears to overestimate the resistance of O_2 diffusion to the particle [5, 16].

Although the ash film concept is widely employed in existing char kinetics models, a macroscopic ash film buildup at the char surface is rarely found [3, 6, 17]. Alternatively, evidence has been found that at typical char combustion temperatures ash mineral components exposed on the surface of the burning char particles can diffuse back into the char matrix itself [3]. The effect of this process of concentration of ash constituents within the char on subsequent char combustion can be modeled as an ***ash dilution*** impact [4, 5], which has been demonstrated to have a dramatic influence on the apparent kinetics reaction order [4]. Recently, considering the possibility of the ash film effect and an ash dilution effect acting in tandem, which is the most realistic scenario, a sophisticated intrinsic kinetics model was developed to predict the ash inhibition during PC char combustion [5]. Char combustion simulations with this model revealed that the ash film influences char combustion throughout its lifetime, whereas ash dilution only inhibits combustion significantly during the final burnout stage [5]. This combined ash inhibition model has been shown to give good predictions for coal and biomass char combustion and gasification [5, 18], as well as the formation of ultra-fine particles during PC char combustion [1, 8].

Several studies have previously analyzed the separate effects of ash volatilization, ash film formation, and ash dilution during PC char combustion. For example, ash vaporization improves pore generation and development [1, 5], ash film formation hinders oxygen transport to the reacting char surface [2, 3, 6], and ash dilution reduces active carbon sites and surface available per unit volume [4, 5]. However, there has been no previous effort to integrate these three distinct ash effects into a thorough mechanistic picture during PC char combustion. Therefore, it is the primary purpose of this work to develop and apply a sophisticated kinetics model, with a focus on the various effects of the three ash evolution mechanisms during PC char combustion in air (O_2/N_2) and oxy-fuel (O_2/CO_2) atmospheres.

2. Model description

An intrinsic kinetics model that considers the combination of ash film and ash dilution effects acting in tandem was developed previously and used to predict ash inhibition during char combustion [5]. Meanwhile, an extended model, named the Char Burning and Particulate Matter Kinetics (CBPMK) model, consisting of the above-mentioned char burning model and an ultra-fine particle formation kinetic model, has been developed and used to model ultra-fine particle formation via ash vaporization during PC char combustion in O_2/N_2 and O_2/CO_2 atmospheres [1, 8]. Although all three ash effects were considered in the CBPMK model, the interactive influences were not considered, in particular the effect of ash vaporization on the char structure and consequently on carbon conversion.

2.1 Intrinsic kinetics model of char combustion

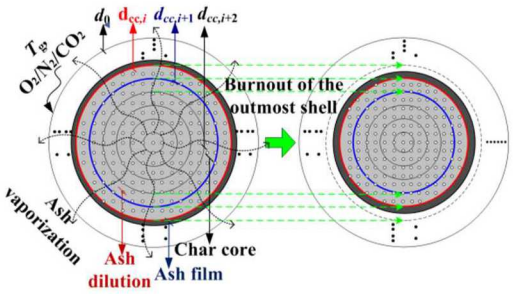

Fig.1 Schematic of the char combustion model with integrated ash effects

As shown in Fig.1, in which the ash effects are integrated into the char combustion model, the initial char particle is divided into numerous equally spaced concentric shells. It is idealized that part of the ash liberated during combustion of each burned shell is used to thicken an ash film on the particle periphery, and the rest is assumed to penetrate and be uniformly distributed in the remaining char core. At the same time, some of the ash vaporizes, depending on the temperature, reducing atmosphere, ash content and components, and physical morphology of the char particle [1, 8, 10]. Any effects of catalysis [3, 19, 20] and char fragmentation [21, 22] are neglected in this model.

In contrast to apparent kinetics models, which are heavily dependent on an empirical mode-of-burning parameter, α, in Eq.1 to describe the gross effects of internal char consumption [2, 4, 23], an intrinsic kinetics approach to carbon conversion is adopted here and used to calculate the unburned carbon mass $m_{\mathrm{c,cc},i+1}$, as described in Eq.2.

$$\rho_{\mathrm{c}}/\rho_{c,0}=(m_{c,cc}/m_{c,0})^{\alpha} \quad \text{(Eq. 1)}$$

$$\frac{m_{\mathrm{c,cc},i}(d_{\mathrm{cc},i+1}/d_{\mathrm{cc},i})^{3}-m_{\mathrm{c,cc},i+1}}{\eta\rho_{\mathrm{c,cc}}S_{\mathrm{g}}d_{\mathrm{cc},i}q_{\mathrm{c,ex}}/6}=\frac{m_{\mathrm{c,cc},i}-m_{\mathrm{c,cc},i+1}}{q_{\mathrm{tot}}} \quad \text{(Eq. 2)}$$

where the outmost shell is numbered i, and the adjacent inner shells are numbered i+1 and i+2, in turn. The overall burning rate, q_{tot}, consisting of both internal and external burning rates of the char, is given by Eq. 3.

$$q_{\mathrm{tot}}=(1-Y_{\mathrm{a,cc}}-\theta_{\mathrm{c,cc}}+\eta\rho_{\mathrm{c,cc}}S_{\mathrm{g}}d_{\mathrm{cc}}/6)q_{\mathrm{c,ex}} \quad \text{(Eq. 3)}$$

where η is the internal effectiveness factor, the ratio of the actual internal burning rate to the maximum possible internal burning rate. The carbon burning rate per unit external surface of char core, $q_{\mathrm{c,ex}}$, is calculated according to the Arrhenius expression shown in Eq.4, which includes oxidation and gasification by both CO_2 and H_2O. More detailed model descriptions of the time-dependent char combustion temperature T_{cc}, carbon density $\rho_{\mathrm{c,cc}}$, internal surface area S_{g}, porosity, diffusion, etc. have been presented in our previous paper [5].

$$q_{\mathrm{c,ex}}=A_{\mathrm{O_2}}\exp(-E_{\mathrm{O_2}}/RT_{\mathrm{cc}})P_{\mathrm{O_2}}^{n_{\mathrm{O2}}}+A_{\mathrm{CO_2}}\exp(-E_{\mathrm{CO_2}}/RT_{\mathrm{cc}})P_{\mathrm{CO_2}}^{n_{\mathrm{CO2}}}+A_{\mathrm{H_2O}}\exp(-E_{\mathrm{H_2O}}/RT_{\mathrm{cc}})P_{\mathrm{H_2O}}^{n_{\mathrm{H2O}}} \quad \text{(Eq. 4)}$$

2.2 Integrated ash effects

As the char particle burns, a portion of the ash mineral vaporizes, and a designated fraction X of the ash liberated after the burnout of each outmost shell is used to form or thicken an ash layer, with the remaining fraction of liberated ash assumed to penetrate uniformly into the char core. By comparing model results with experimental char combustion temperatures and burnout over a range of combustion conditions for a high-volatile bituminous coal, a value of 0.16 was recommended for the presumed fraction of liberated ash forming an ash film [5]. While this value of X has been empirically determined, it is expected that the ash fusion temperature and char combustion temperature, which together influence the ash flowability in the char, should have important effects on the ash disposition. Here, a range of 0.075-0.3 is assumed for X, which brackets the empirically determined value.

A mass balance on ash in the ash film is expressed as Eq.5.

$$\rho_{\mathrm{a,n}}\left(1-\theta_{\mathrm{a,f}}\right)\left[\left(2\delta+d_{\mathrm{cc},\,i+1}\right)^3-d_{\mathrm{cc},\,i+1}^3\right]\pi/6=X\left(d_{\mathrm{cc},\,i}^3-d_{\mathrm{cc},\,i+1}^3\right)\left(Y_{\mathrm{a},i}\rho_{\mathrm{cc},i}\,\pi/6-V_{\mathrm{vap},i}\Delta t/d_{\mathrm{cc},\,i}^3\right)+m_{\mathrm{af},i} \qquad \text{(Eq.5)}$$

where the left-hand side is the ash film mass for shell i+1 after the burnout of char shell i, the first term on the right-hand side accounts for the newly added ash film mass (excluding vaporization and accounting for the fraction X of the liberated mass contributing to the ash film), and the second term on the right-hand side accounts for the inherited mass of the ash film from shell i. $\rho_{\mathrm{a,n}}$ and $\theta_{\mathrm{a,f}}$, representing the nonporous ash density and ash porosity, are assumed to be 2.65×10^3 kg/m^3 and 0.25, respectively [2]. δ, $Y_{\mathrm{a}.i}$, and $\rho_{\mathrm{cc},i}$ are the time-dependent ash film thickness, ash content in the char, and char density in the char core, respectively. $V_{\mathrm{vap},i}$ is the instantaneous vaporization rate of included minerals.

The vaporization rate is calculated by assuming that all ash minerals are uniformly distributed as oxide inclusions (MO_n) throughout the char matrix and vaporize in the forms of sub-oxides or fully reduced metals (MO_{n-1}) according to R1 [1, 8, 10]. SiO_2 is employed as representative of the refractory oxides.

$$MO_n(\mathrm{s,l})+CO\rightarrow MO_{n-1}(\mathrm{g})+CO_2 \qquad \text{(R1)}$$

Based on vapor diffusion within the porous char, the mineral vaporization rate, V_{vap}, can be given as Eq. 6,

$$V_{\text{vap}} = \eta' N_{\text{MO}_n} 4\pi r_{\text{MO}_n} D_{\text{eff}} P^{\text{eq}}_{\text{MO}_{n-1}} / RT_{\text{cc}} \qquad \text{(Eq. 6)}$$

where r_{MO}, N_{MO}, and P_{M}^{eq} are the inclusion radius, number, and partial pressure of the suboxide or reduced metal, as computed through reaction R1. The effectiveness factor η' is the ratio of the total vaporization rate of inclusions to the vaporization rate of N_{MO} isolated inclusions. The effective Knudsen diffusivity D_{eff} is calculated according to Eq. 7, wherein the ratio of the tortuosity to the constriction factor of the pores, τ/σ_c, is assumed to be 6 [22].

$$D_{\text{eff}} = 9700\bar{r}\left(\frac{T_{\text{cc}}}{M_{\text{MO}_{n-1}}}\right)^{0.5} \frac{\sigma_c}{\tau}\left(\frac{\theta_{a,f} V_{a,cc}}{V_{\text{cc}}} + \frac{\theta_c V_{c,cc}}{V_{\text{cc}}}\right) \qquad \text{(Eq. 7)}$$

N_{MO}, the number of isolated inclusions within the char matrix, is a function of the transient char particle size, $d_{\text{cc},i}$, and the volume fraction of inclusions in the char, θ', and is given by Eq. 8.

$$N_{\text{MO}_n} = \theta'\left(0.5 d_{\text{cc},i} / r_{\text{MO}_n}\right)^3 \qquad \text{(Eq. 8)}$$

θ' is calculated according to Eq.9, where $F_{\text{MO}n}$ and $m_{\text{a},0}$ are the initial mass fraction of the inclusion in the ash and the initial ash mass, and $F_{\text{MO}n,i}$ and $m_{\text{af},i}$ are the transient mass fraction of inclusion in the ash film and the ash film mass when shell i+1 begins to burn.

$$\theta' = 6\left(F_{\text{MO}_n} m_{a,0} - \sum_{j=0}^{j=i}\left(V_{\text{vap}}\Delta t\right)_j - F_{\text{MO}_n,i} m_{\text{af},i}\right) \Big/ \rho_{\text{MO}} \pi d^3_{\text{cc},i} \qquad \text{(Eq. 9)}$$

2.3 Kinetic parameters selection and modeling conditions

We employ the same kinetic parameters as used as in our previous papers [1, 5, 8], wherein the char burning characteristics and the vaporization rates of different inclusions predicted by the kinetic models were found to compare favorably with available experimental data. The pre-exponential factor is 8.0 kg/s/cm^2/atm$^{0.1}$ for the oxidation reaction and 5.0 kg/s/cm^2/atm$^{0.5}$ for gasification by CO_2, and the corresponding activation energies are 150 kJ/mol and 251 kJ/mol. The intrinsic reaction order for reaction with oxygen is assumed to be 0.1 and for reaction with CO_2 is 0.5. The H_2O gasification reaction is ignored. The investigated combustion parameters span a wide range, as summarized in Table 1, to evaluate the variation in ash effects as a function of char characteristics and combustion conditions.

Table 1 Summary of simulation conditions

Parameters	Symbol	Unit	Nominal value	Minimum	Maximum
Gas temperature	T	K	1650	1500	1800
O_2 content	O_2	vol.%	21	12	27
Char particle size	d	μm	65	40	90
Ash content	F_a	wt.%	15	5	25
Inclusion content	F_{inc}	wt.%	30	10	90
Ash film fraction	X	wt.%	15	7.5	30

3. Results and discussion

3.1 Ash distribution under various combustion conditions

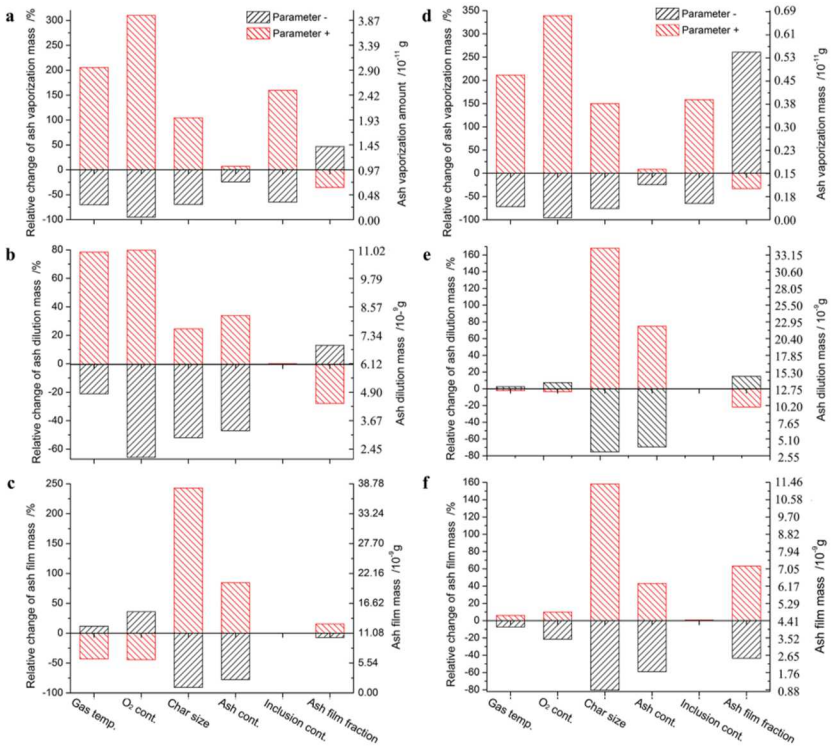

Fig.2 Distribution of ash vaporization, ash dilution, and ash film under various combustion conditions in O_2/N_2 (a, b, and c) and O_2/CO_2 (d, e, and f) atmospheres

Fig.2 shows the mass distribution of ash vaporization, ash dilution, and ash film under various combustion

conditions in O_2/N_2 and O_2/CO_2 atmospheres (according to the parameter set shown in Table 1) at the point of 99% consumption of the char carbon. It can be seen from Figs. 2a and 2d that in both O_2/N_2 and O_2/CO_2 atmospheres the ash vaporization mass increases with increasing combustion gas temperature, O_2 content, char size, ash content, and evaporable inclusion content, as well as decreasing ash film forming fraction. Elevated combustion gas temperature and O_2 content causes higher char burning temperatures, which elevate both the vapor diffusion efficiency (D_{eff}', Eq.7) and the vapor equilibrium partial pressure (P_M^{eq}, Eq.6), leading to greater vaporized ash mass. Increasing char size, ash content and inclusion content increase the inclusion number (N_{MO}, Eq.8) and inclusion volume (θ', Eq.9) and consequently ash vaporization, though the lower char combustion temperature with a high ash content almost neutralizes the effect of the added ash content on the amount of vaporized ash. An increased ash film fraction not only reduces the amount of ash dilution and resultant inclusion content but also reduces the char combustion temperature [5] and therefore decreases the amount of ash vaporization. Note that the total amount of ash vaporization during combustion in O_2/CO_2 atmospheres is lower than that in O_2/N_2 atmospheres by about a factor of six, due to the much lower char combustion temperatures in O_2/CO_2 atmospheres [1, 24, 25].

In O_2/N_2 atmospheres, as shown in Figs. 2b and 2c, the ash dilution mass increases at high gas temperature and O_2 content, whereas the ash film mass decreases. High gas temperature causes high char burning temperature, which not only improves the external char conversion rate ($q_{c,ex}$, Eq.4) but also significantly accelerates char internal reaction rate through the effectiveness factor (η, Eq.3), thereby favoring ash dilution. Similarly, an elevated O_2 content in the bulk gas causes a higher char burning temperature and greater O_2 diffusion into the char matrix, thus improving the internal char conversion rate.

In contrast, in O_2/CO_2 atmospheres increasing the gas temperature and O_2 content produce opposite trends in the ash dilution mass and ash film mass as those in O_2/N_2 atmospheres, as shown in Figs. 2e and 2f. This result is due to the strong internal diffusion control of the CO_2 gasification reaction and external diffusion control of oxidation reaction [25], such that increasing the gas temperature and the O_2 content promotes the external reaction

of the char matrix slightly more than the internal reaction, consequently increasing ash film mass and decreasing ash dilution mass. Because of the strong role of internal reaction in O_2/CO_2 atmospheres, the residual ash mainly exists within the char matrix as dilution ash rather than an external ash film, which is dominant in O_2/N_2 atmospheres. Indeed the amount of dilution ash is larger by over a factor of two for oxy-fuel combustion relative to combustion in air.

In both O_2/N_2 and O_2/CO_2 atmospheres, increasing the char particle size and ash content results in growth of both ash film and dilution ash, because these factors increase the total amount of ash in the particle. As expected, an increase in the presumed ash film forming fraction increases the mass of ash in the external ash film and decreases the ash dilution mass. A change in the volatile inclusion content shows no tangible effect on the mass distribution of the ash film and ash dilution, due to the much lower mass of vaporized ash, which is approximate 3 orders less than the mass of ash dilution and the ash film.

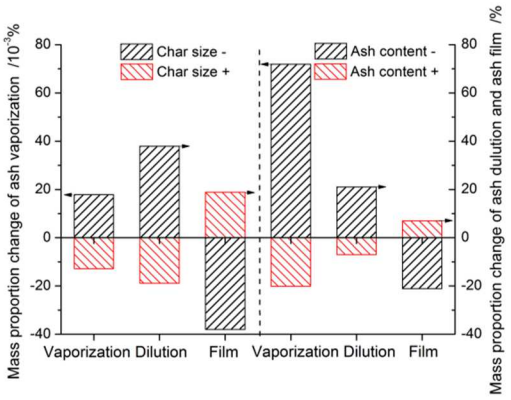

Fig.3 Changes in the ash distribution during combustion with different char particle sizes and ash contents in O_2/N_2

Although an increasing char particle size and increasing ash content cause an increase in the mass of ash vaporization, ash dilution, and ash film (Fig.2), an examination of the relative ash mass distribution in response to these factors gives insightful trends. As shown in Fig.3, both a larger char particle size and higher ash content, which result in a lower char burning temperature [5] and hinder the diffusion of mineral vapor towards the char surface, result in a decreasing ash vaporization fraction. The mass proportion of ash dilution decreases with larger

char size and higher ash content. This is due to the hindered oxygen diffusion within the particle from these factors, resulting in a lower internal reaction rate relative to the external reaction rate. It is clear from these examples that the global combustion environment (temperature and atmosphere) and char properties (size, ash content, evaporable inclusion content) have important effects on ash evolution and distribution.

3.2 Effects of ash distribution on char conversion

Fig.4 shows the effects of ash vaporization and ash film forming fraction X (or ash dilution fraction, 1 - X) on the char conversion characteristics (with a carbon conversion ratio of 99 wt.%) under the nominal combustion condition. The ash distributions, especially the ash film and ash dilution, significantly affect the char conversion characteristics, including the burnout time and the structure of the residual ash particle (i.e. the thickness of the external ash film and the size of the internal residual char core).

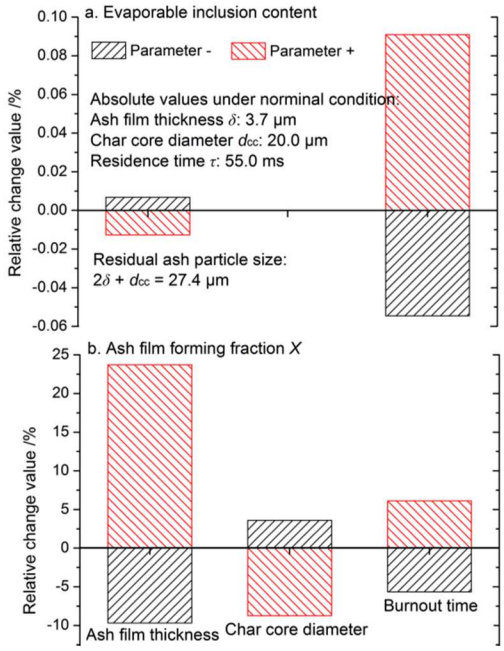

Fig.4 Effects of ash vaporization and ash film (or ash dilution) forming fraction on char conversion in O_2/N_2

As shown in Fig.4a, a high vaporizable inclusion content causes a slightly thinner ash film and slightly longer burnout time, while there is no impact on the size of the internal residual char core. A high ash film forming fraction causes a thick ash film, a small residual char core size, and a longer burnout time, as shown in Fig.4b. The ash distributions do not impact the residual ash particle size, which remains unchanged at 27.4 μm, but the residual

ash particle is encased by a thick film when the ash film forming fraction is high. High fractions of ash vaporization and ash film forming fraction extend the burnout time, whereas high ash dilution fraction shortens the burnout time.

3.3 Importance of combined ash effects

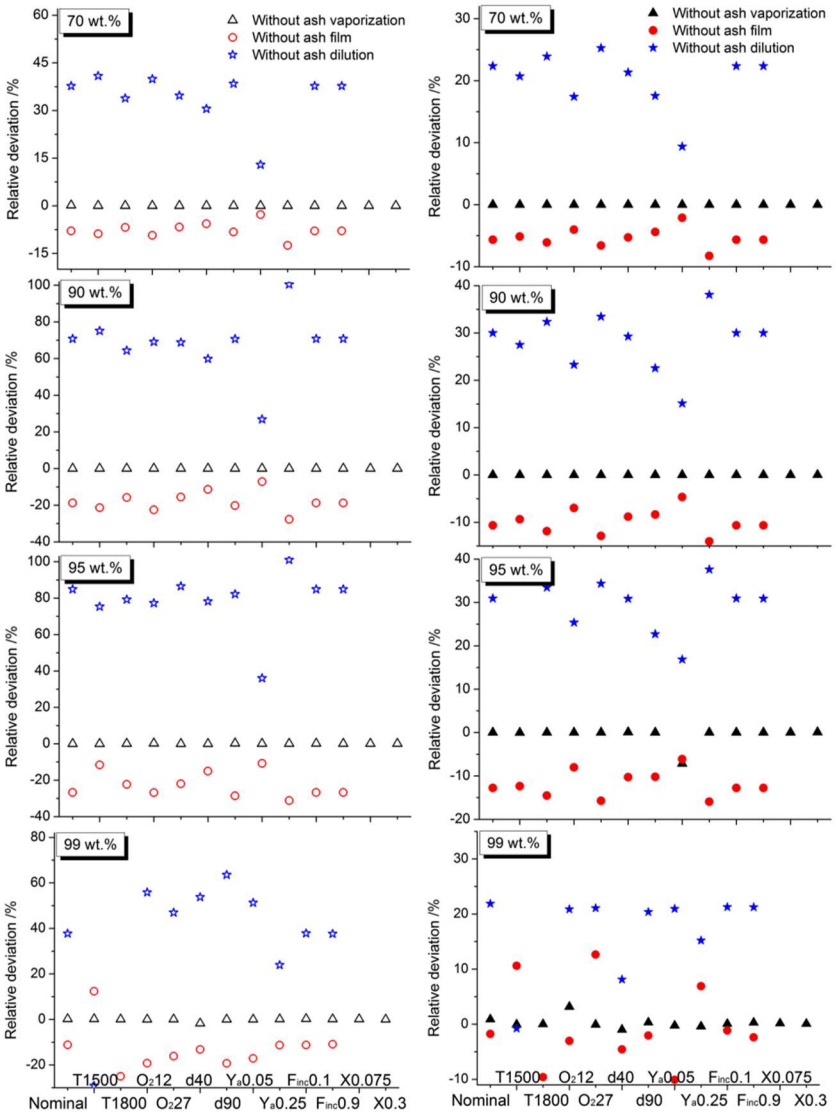

Fig.5 Effects of the different ash evolution routes on the char burnout time at different extents of carbon conversion (left panel: O_2/N_2; Right panel: O_2/CO_2). The x-axis indicates the different range limit values for the variables listed in Table 4 that were considered for each simulated combustion condition.

Fig. 5 shows the quantitative effects of the ash distribution on the char burnout time under different combustion conditions at 70, 90, 95, and 99 wt.% carbon conversion. In O_2/N_2 atmospheres, the relative deviation from the nominal combustion condition is between -1.8 — +0.3% when ignoring ash vaporization, -32— +13%

when ignoring ash film formation, and -30 — +101% when ignoring ash dilution. Due to the stronger influence of internal char conversion in O_2/CO_2 atmospheres, and thus the possibility of high CO/CO_2 ratio improving inclusion reduction and vaporization (R1), the importance of ash vaporization (-7.2 — +3.2%) is greater than in O_2/N_2 atmospheres. However, because of the lower combustion temperatures in O_2/CO_2 atmospheres, the impact of the external ash film (-16 — +13%) and ash dilution (-0.8 — +38%) is less than in O_2/N_2 atmospheres. In both atmospheres, as the carbon conversion ratio increases from 70 wt.% to 99 wt.%, the relative deviations caused by the ash film and ash dilution first increase and then decrease, whereas the relative deviation from ash vaporization consistently increases.

4. Conclusions

A sophisticated intrinsic char kinetics model that includes ash vaporization, external film formation, and ash dilution effects within pulverized coal char particles has been developed and is used here to investigate the combined ash effects on PC char conversion during air (O_2/N_2) and oxy-fuel (O_2/CO_2) combustion. Both in O_2/N_2 and O_2/CO_2 atmospheres, the ash vaporization mass increases with increasing combustion gas temperature, O_2 content, char particle size, ash content, and evaporable inclusion content, whereas it decreases with increasing ash film forming fraction. In O_2/N_2 atmospheres, higher gas temperature and O_2 content cause increasing ash dilution mass and decreasing ash film mass. However, they show the opposite effects in O_2/CO_2 atmospheres. The residual ash mainly exists as dilution ash in O_2/CO_2 atmospheres because of the internal diffusion control of CO_2 gasification, rather than ash film, which is dominant in O_2/N_2 atmospheres because of the external diffusion control of oxidation. Although large char particle size and high ash content increase the mass of all ash constituents, the proportions of ash vaporization and ash dilution decrease, and the ash film proportion increases. For the case of SiO_2 ash modeled here, the mass of ash vaporization is approximate three orders less than the mass of ash associated with ash dilution and an external ash film, and the ash vaporization in O_2/CO_2 atmospheres is lower than that in O_2/N_2 atmospheres by about a factor of six due to the lower char combustion temperatures in O_2/CO_2

atmospheres.

Despite the minor amount of refractory ash that is vaporized, it can still influence the char conversion rate by up to nearly 10% for oxyfuel combustion conditions. In both O_2/N_2 and O_2/CO_2 atmospheres, the influence of the three modeled ash phenomena on char burnout time follows the order: ash dilution ＞ ash film ＞ ash vaporization. With increasing carbon conversion, the importance of ash vaporization increases, whereas the importance of ash film and ash dilution first increase and then decrease.

Acknowledgements

The present work was supported by National Natural Science Foundation of China (51776161). Sandia National Laboratories is a multimission laboratory managed and operated by National Technology and Engineering Solutions of Sandia, LLC., a wholly owned subsidiary of Honeywell International, Inc., for the U.S. Department of Energy's National Nuclear Security Administration under contract DE-NA-0003525.

References

[1] Y.Q. Niu, S. Wang, C.R. Shaddix, S.E. Hui, Combust. Flame 173 (2016) 195-207.

[2] R. Hurt, J.K. Sun, M. Lunden, Combust. Flame 113 (1-2) (1998) 181-197.

[3] M.M. Lunden, N.Y.C. Yang, T.J. Headley, C.R. Shaddix, Symp. Int. Combust. 27 (2) (1998) 1695-1702.

[4] J.J. Murphy, C.R. Shaddix, Combust. Flame 157 (3) (2010) 535-539.

[5] Y.Q. Niu, C.R. Shaddix, Proc. Combust. Instit. 35 (1) (2015) 561-569.

[6] R.H. Hurt, K.A. Davis, Symp. Int. Combust. 25 (1) (1994) 561-568.

[7] Y.L. Jia, J.S. Lighty, Environ. Sci. Technol. 46 (9) (2012) 5214-5221.

[8] Y. Niu, X. Liu, S. Wang, S.e. Hui, C.R. Shaddix, Combust. Flame 184 (2017) 1-10.

[9] C.M. Lee, K.A. Davis, M.P. Heap, E. Eddings, Proc. Combust. Instit. 28 (2) (2000) 2375-2382.

[10] M. Neville, R. Quann, B. Haynes, A. Sarofim. Symp. Int. Combust. 18 (1) (1981) 1267-1274.

[11] Y.Q. Niu, H.Z. Tan, S.E. Hui, Prog. Energ. Combust. 52 (2016) 1-61.

[12] J.K. Sun, R.H. Hurt, Proc. Combust. Instit. 28 (2) (2000) 2205-2213.

[13] S. Jayanti, K. Maheswaran, V. Saravanan, Appl. Math. Model. 31 (5) (2007) 934-953.

[14] R.C. Everson, H. Neomagus, G.W. van der Merwe, A. Koekemoer, J.R. Bunt, Fuel 140 (2015) 17-26.

[15] S. Niksa, Y. Sakurai, N. Fujiwara, Energ. Fuel. 31 (4) (2017) 4507-4519.

[16] M. Cloke, T. Wu, R. Barranco, E. Lester, Fuel 82 (15-17) (2003) 1989-2000.

[17] R. Hurt, K. Davis, Combust. Flame 116 (4) (1999) 662-670.

[18] T. Li, Y. Niu, L. Wang, C. Shaddix, T. Løvås, Appl. Energ. (2017).

[19] H. Watanabe, K. Okazaki, Proc. Combust. Instit. 35 (2) (2015) 2363-2371.

[20] Z.Z. Zhang, M.M. Zhu, Y. Zhang, H.Y. Setyawan, J.B. Li, D.K. Zhang, Proc. Combust. Instit. 36 (2) (2017) 2139-2146.

[21] R.E. Mitchell, A.E.J. Akanetuk, Symp. Int. Combust. 26 (2) (1996) 3137-3144.

[22] L.L. Baxter, Coal char fragmentation during pulverized coal combustion, Report No. SAND-8250c, UC-1409, Sandia National Laboritories, 1995.

[23] R.E. Mitchell, L.Q. Ma, B. Kim, Combust. Flame 151 (3) (2007) 426-436.

[24] M. Geier, C.R. Shaddix, K.A. Davis, H.-S. Shim, Appl. Energ. 93 (2012) 675-679.

[25] E.S. Hecht, C.R. Shaddix, M. Geier, A. Molina, B.S. Haynes, Combust. Flame 159 (11) (2012) 3437-3447.

Figure captions

Fig.1 Schematic of the char combustion model with integrated ash effects

Fig.2 Distribution of ash vaporization, ash dilution, and ash film under various combustion conditions in O_2/N_2 (a, b, and c) and O_2/CO_2 (d, e, and f) atmospheres

Fig.3 Changes in the ash distribution during combustion with different char particle sizes and ash contents in O_2/N_2

Fig.4 Effects of ash vaporization and ash film (or ash dilution) forming fraction on char conversion in O_2/N_2

Fig.5 Effects of the different ash evolution routes on the char burnout time at different extents of carbon conversion (left panel: O_2/N_2; Right panel: O_2/CO_2). The x-axis indicates the different range limit values for the variables listed in Table 4 that were considered for each simulated combustion condition.